

# Numerical study of turbulence over a receding wall by controlled and thermal ablation

By R. Crocker<sup>†</sup> AND Y. Dubief<sup>†</sup>

The numerical simulation of turbulent flow over a receding wall is investigated for the development of a direct numerical simulation(DNS) algorithm for low-temperature ablation. The algorithm combines level-set methods to define the motion of the fluid-solid interface and immersed boundary methods to simulate the presence of solid on non-conforming mesh. The first study is a numerical experiment in which the wall recession is imposed in a periodic turbulent channel flow. The response of turbulence as a function of the recession velocity is investigated, with a focus on non-equilibrium effects and predictability. For instance, it is found that turbulence remains at equilibrium when the recession velocity is 1% of the skin-friction velocity before onset of recession. When the recession velocity is equal to the skin-friction velocity, strong non-equilibrium effects appear, with the noticeable formation of a shear layer. The second study deals with wall recession caused by thermal ablation. The objective to assess the robustness of our algorithm for locally large ablation velocity. Large ablation velocity compounded by significant differences in the thermodynamical properties of the fluid and solid may result in numerical instabilities that cause the divergence of the flow and thermal solutions. The problem is remediated by using virtual ghost points for the treatment of temperature derivatives at the interface and a control loop that constrains the time-step based on the maximum ablation velocity.

---

## 1. Introduction

The complex interaction between eroding turbulence and an eroded wall (here erosion is used to encompass all eroding processes including ablation) has surprisingly received little attention in the fluid mechanics community. The proposed research is motivated by the fact that upon onset of ablation, models do not exist that can predict the cascading interactions between a flow and a receding surface. The present study is focused on the fundamental investigation of the dynamical interactions between an ablating flow and an ablated wall using fixed and thermally driven ablation velocities. Fixed ablation velocities are used as a numerical experiment to decouple the response of wall turbulence to a receding wall. Thermal ablation simulations are performed for low-temperature materials such as wax. The objective of this brief is to investigate the numerical challenges inherent in the strong variations in density and thermodynamical properties across the fluid-solid interface.

Conceptually, flow-induced erosion may be considered as a branch of reacting flows due to the mechanical, thermodynamic or chemical coupling between erosive flow and erodible wall resulting in the modification of mass, structure and/or chemistry of both flow and wall. While significant progress has been made in the simulation of multiphysics in the context of turbulent flows (see Moin & Iaccarino 2007, for applications to multiphase

<sup>†</sup> School of Engineering and Vermont Advanced Computing Center, University of Vermont

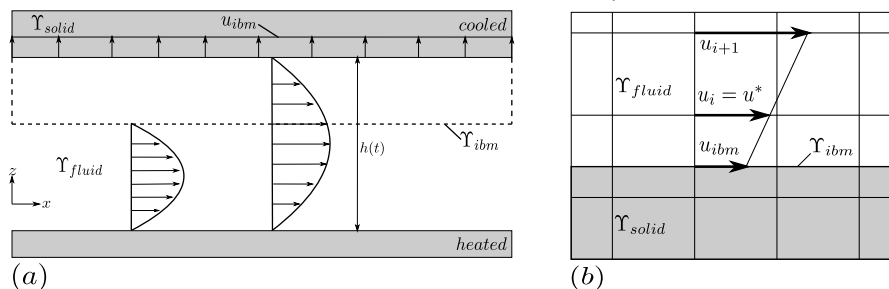


FIGURE 1. (a) Schematic of the total domain with the IB separating the fluid and solid domains.  $h(t)$  is the instantaneous channel height uniform through out the domain for section 3.1 but can vary as a function of  $x_1$  during ablation, section 3.2. The dotted line represents the position of the wall before recession. (b) Linear interpolation stencil along IB.

flows and combustion), the simulation and prediction of erosion is mostly limited to slow erosion processes, i.e., when the time scale of erosion is much greater than the typical time scale of turbulence, making equilibrium turbulence models (e.g., Reynolds Average Navier-Stokes models, or RANS) applicable. For rapid erosion processes, the challenge resides in the simultaneous resolution of constantly evolving (non-equilibrium) turbulence and walls due to the erosion process. Non-equilibrium (regimes where closure models such as RANS no longer apply) turbulence requires numerical techniques that can capture the time and space evolution of turbulent structures, which is best accomplished by direct numerical simulation (DNS) or large eddy simulations. Due to the fundamental nature of the project, the former numerical strategy is adopted and coupled with level set and immersed boundary methods to describe the evolution of the ablated wall's interface. Immersed boundary methods (IB) have the distinct advantage of simulating the presence a solid region on a flow computational domain without the numerical expense of body fitting the computational grid and remeshing for moving walls (Mittal & Iaccarino 2005). Level set methods (Osher & Sethian 1988) are used to capture the sharp interface solid-fluid and its evolution during ablation.

The ablative flow and ablated walls are confined between two horizontal, isothermal walls with periodic conditions in horizontal directions. The set-up allows for the simulation of natural and forced convection. The first study focuses on the treatment of temperature at the fluid-solid interface. The simulated physics is reduced to an ideal case, where the density of the ablated wall and ablative fluid are equal, thus removing the transport equation of mass. The proposed system approaches ablation of  $\text{CO}_2$ (dry-ice) by hot  $\text{CO}_2$ (gas).

## 2. Methods

### 2.1. Flow configuration

Figure 1 is a sketch of the computational domain. The bottom plate is isothermal and heated at temperature  $T_{\text{hot}}$  and the top plate is cooled at temperature  $T_{\text{cold}}$ . For future scaling considerations, the temperature gradient is denoted by  $\Delta T = T_{\text{hot}} - T_{\text{cold}}$ . Periodic boundary conditions are applied in horizontal directions,  $x_1 = x$  and  $x_2 = y$ . Gravity  $g$  is applied in the vertical direction  $x_3 = z$ ,  $g_i = -g\delta_{i3}$ . Throughout this document, Einstein's index notation is used, and  $\delta_{ij}$  is the Kronecker tensor.

The ablated wall is attached to the cold wall, as shown in figure 1a. The fluid and solid domains are denoted  $\Upsilon_{\text{fluid}}$ , and  $\Upsilon_{\text{solid}}$ , respectively. The height  $h(t)$  defines the averaged

distance of the fluid-solid interface from the hot wall denoted as  $\Upsilon_{\text{ibm}}$ . As discussed later, the wall boundary condition at the surface of the ablated wall is enforced by an immersed boundary method (IBM), which consists of the corrected velocity and temperature at nodes in the immediate vicinity of the surface or at the surface, based on the surface velocity and temperature. The IB method is sketched in figure 1b for the velocity  $u_i$  using linear interpolation.

### 2.2. Governing Equations

The fluid-solid interface is defined by the zero isosurface of the level set variable  $G$ , whose transport is governed by the local ablation velocity at the wall:

$$\frac{\partial G}{\partial t} + v_a \left| \frac{\partial G}{\partial x_i} \right| = 0. \tag{2.1}$$

In the solid domain,  $G$  is positive, and negative in the fluid so that the surface normal is always directed to the solid surface. Also,  $G$  is maintained as a distance function, i.e.  $|\partial G/\partial x_i| = 1$ , through periodic application of a redistancing procedure. The ablation velocity  $v_a$ , defined later, is therefore positive wherever ablation is to occur. The heat equation, under the hypothesis of incompressibility, may be reduced to the following non-dimensional form:

$$\frac{\partial T}{\partial t} + \mathcal{H}(-G) \frac{\partial}{\partial x_i} (u_i T) = \frac{\partial}{\partial x_i} \left( \frac{1}{RePr(G)} \frac{\partial T}{\partial x_i} \right), \tag{2.2}$$

where  $\mathcal{H}$  is the Heaviside function and the Prandtl number is the ratio of fluid viscosity  $\nu$  to the thermal diffusivity  $\alpha$ , locally determined by the sign of  $G$ . The Reynolds is based on the half-height  $h_0$  of the fluid domain, and skin friction velocity  $u_{\tau_0}$  prior to the onset of ablation. The dimensional temperature  $\tilde{T}$  is normalized by the melting temperature of the wall  $T_m$  and the temperature at the hot wall,  $T_{\text{hot}}$ ,  $T = (\tilde{T} - T_m)(T_{\text{hot}} - T_m)$ . Using the Boussinesq approximation for the buoyancy force, the flow equations are:

$$\frac{\partial u_i}{\partial x_i} = 0, \tag{2.3}$$

$$\frac{\partial u_i}{\partial t} + \frac{\partial u_i u_j}{\partial x_j} = -\frac{\partial p}{\partial x_i} + \frac{1}{Re} \frac{\partial}{\partial x_j} \left( \frac{\partial u_j}{\partial x_i} \right) + \frac{Gr}{Re^2} T \delta_{i3} - \frac{dP}{dx_1} \delta_{i1} + f_i^{\text{ibm}}, \tag{2.4}$$

where  $u_i$  and  $p$  are the non-dimension velocity vector and pressure. The mean pressure gradient  $-dP/dx_1$  is set to unity for forced convection flows and zero for natural convection. The velocity scale used to normalize the channel flow ( $u_i$  and  $p$ ) is  $u_{\tau_0}$ . In the case of natural convection (a majority of the velocity occurs in the  $x_3$  direction due to convection), the Reynolds number can be shown to be  $Re = \sqrt{Gr}$ , where the Grashof number is  $Gr = \beta \Delta T h_0^3 g / \nu^2$ . Here  $\beta$  is the expansion coefficient of the fluid. The additional force  $f_i^{\text{ibm}}$  in Eq. 2.4 enforces the immersed boundary method at the fluid-solid interface:  $f_i^{\text{ibm}} = 0$  in  $\Upsilon_{\text{fluid}}$  and  $f_i^{\text{ibm}} \neq 0$  at  $\Upsilon_{\text{ibm}}$  and  $\Upsilon_{\text{solid}}$ . In the solid,  $f_i^{\text{ibm}}$  is determined to achieve  $u_i = 0$ , whereas at the interface,  $f_i^{\text{ibm}}$  is computed to enforce a surface velocity that satisfies mass-conservation and the surface velocity.

### 2.3. Discretization

Eqs. 2.3 and 2.4 are discretized using the fractional step method (Kim & Moin 1985).

$$\frac{u_i^{n+1/2} - u_i^n}{\Delta t} = -\gamma_n N_i^n - \zeta_n N_i^{n-1} + \alpha_n (L_i^{n+1} + L_i^n) \tag{2.5}$$

$$\frac{\partial}{\partial x_k} \frac{\partial}{\partial x_k} \phi = \frac{1}{\alpha_n \Delta t} \frac{\partial u_k^{n+1/2}}{\partial x_k} \quad (2.6)$$

$$u_k^{n+1} = u_k^{n+1/2} - \alpha_n \Delta t \frac{\partial \phi}{\partial x_k}, \quad (2.7)$$

where  $L$ , and  $N$  are, respectively, the diffusive, and convective terms for a centered finite difference discretization of Eq. 2.4,  $\phi$  is the pseudo pressure,  $\gamma_n$ ,  $\zeta_n$ ,  $\alpha_n$  are the third-order Runge-Kutta coefficients, and  $n$  is the time-step. Velocity and pressures are stored on a staggered grid, uniform in horizontal directions and stretched in the vertical directions to ensure adequate resolution in near-wall regions. Eq. 2.5 is advanced in time with a semi-implicit third-order Runge-Kutta/second-order Crank Nicolson method. The code used to solve Eqs. 2.5-2.7 has been previously validated in Dubief *et al.* (2005). By grouping  $L$  and  $N$  into  $RHS$ , Eq. 2.5 can be rewritten with the addition of  $f_i^{\text{ibm}}$ .

$$\frac{u_i^* - u_i^n}{\Delta t} = RHS^{n+1/2} + f_i^{\text{ibm}}. \quad (2.8)$$

$u_i^*$  is the linearly interpolated velocity at the node on the fluid side of the IB;  $u^* = w_i u_{i+1} + u_{\text{ibm}}$ , where  $w_i$  is the appropriate linear interpolation coefficient (see figure 1b). The forcing term from Eq. 2.8 is added to the  $RHS$  of Eq. 2.5 enforcing the boundary condition at the IB at time  $n + 1$ . This application of the forcing at an IB is explained in detail in Mohd-Yusof (1997). The immersed boundary velocity is controlled by the Stephan condition (except for section 3.1).

$$v_a = u_{\text{ibm}} = \frac{Ste}{Re Pr_f} \frac{\rho_s}{\rho_f} \left( \frac{\kappa_s}{\kappa_f} \frac{\partial T_s}{\partial x_i} - \frac{\partial T_f}{\partial x_i} \right) n_i \text{ if } T_{\text{ibm}} \geq T_m. \quad (2.9)$$

$Ste$  is the Stephan number,  $Pr_f$  is the Prandtl numbers of the fluid,  $T_s$ ,  $T_f$ , and  $\kappa_s$ ,  $\kappa_f$  are the temperatures and thermal conductivities on the solid and fluid sides respectively, and  $n_i = \partial G / \partial x_i$  is the surface normal. While  $T_{\text{ibm}} \geq T_m$  holds temperature continuity across the interface is enforced but the total flux across the interface will not be zero. If  $T_{\text{ibm}} < T_m$  conjugate heat transfer is assumed and  $u_{\text{ibm}} = 0$ , phase change occurs only from solid to fluid, not vice versa.

$$T_s = T_f = T_{\text{ibm}} \text{ and } \frac{\kappa_s}{\kappa_f} \frac{\partial T_s}{\partial \vec{n}} = \frac{\partial T_f}{\partial \vec{n}}. \quad (2.10)$$

The conditions in Eq. 2.10 cannot be satisfied simultaneously so they are approximated using an iterative method. The Dirichlet condition is applied to the solid side of the interface and the Neumann condition is applied to the fluid side of the interface (Kang *et al.* 2009). In Eq. 2.2, the large discontinuity in temperature gradients across the interface requires the implicit treatment of the diffusive term in three dimensions, due to the potential three-dimensionality of ablated surfaces. This is achieved using approximate factorization coupled with an interactive procedure for the update of velocity and temperature near the interface. For an error of  $10^{-6}$ , on average 3 to 4 iterations are typically needed during fast ablation. IB forcing for temperature is applied to the discretized Eq. 2.2 by adding ghost points at the interface (Tseng 2003). Ghost points keep the temperature field continuous and effectively decouple the solution matrices of the fluid and solid domains. Thermal communication between the two domains is controlled through equations 2.9 or 2.10.

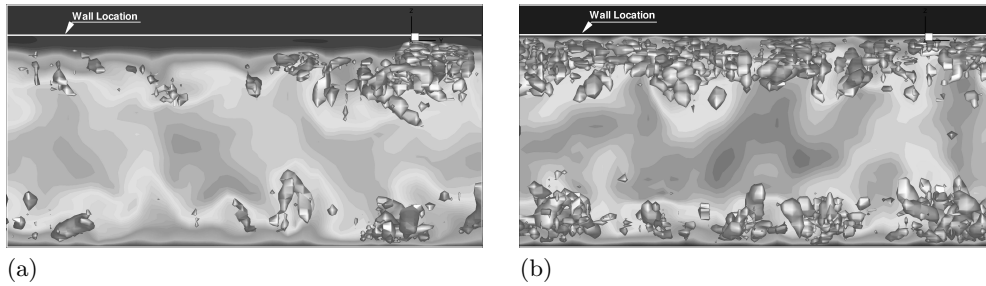


FIGURE 2. (a) Snapshot of the flow for a controlled wall recession at  $v_a = u_{\tau 0}$ . Vortices (isosurfaces of  $Q = 100$ ) and streamwise velocity  $u$  contours are shown in a cross section perpendicular to the flow. (b) Same as in (a) for  $v_a = 0.01u_{\tau 0}$ .

### 3. Results

#### 3.1. Isothermal wall recession

The first set of simulations study the response of a turbulent channel flow to a receding wall. The motivation here is to decouple the flow dynamics to the wall dynamics by controlling the latter. Here, the ablated wall is moved at constant speed, while the pressure gradient is kept constant. This numerical experiment is also a good test of the robustness of our method. Using the computational domain sketched in figure 1, a low Reynolds number channel flow is first established at  $Re = 125$  in a fluid domain of dimensions  $L_x = 10$ ,  $L_y = 5$ ,  $L_z^{\text{channel}} = 2$ . The resolution is  $N_x = 64$ ,  $N_y = 64$ ,  $N_z^{\text{channel}} = 65$ . The wall is mapped by a uniform grid consisting of  $N_z^{\text{wall}} = 250$  in the wall-normal direction, with a grid spacing of  $\Delta_z^+ = 0.25$  based on  $u_{\tau 0}$ . The above resolution are set at the beginning of the experiment, as the wall recedes the amount of computational nodes increases in  $N_z^{\text{channel}}$  and decreases in  $N_z^{\text{wall}}$ . To conserve mass a velocity boundary condition equal and opposite to  $v_a$  is added to the fluid domain at  $\Upsilon_{\text{ibm}}$ . Due to the non-equilibrium nature of the flow, only snapshot statistics, i.e., space averaged in horizontal directions, are discussed. Two fixed ablation velocities are considered:  $v_a = u_{\tau 0}$  and  $v_a = 0.01u_{\tau 0}$ . In these simulations, the temperature field is decoupled from the momentum by assuming that the wall and fluid are isothermal. To illustrate the difference between fast and slow wall recession, the following visualizations and statistics are extracted from the time at which the flow domain is increased by 10% (40% of wall loss). The vortical activity of each flow is shown in figures 2a and 2b along with contours of the streamwise velocity component. The fast ablation creates a region of low speed fluid, clearly seen in figure 2a. At this point of the simulation, vortical structures, identified by isosurfaces of positive second-invariant  $Q$  of the velocity gradient tensor, show signs of weakening caused by the sudden expansion. Due to the low Reynolds number of the simulation, the influence of the sudden expansion is communicated to the non-moving (lower) wall and results also in a weakening of the vortical structures. For larger wall loss (not shown here), the near-wall region adopts a shear layer structure with the formation of Kelvin-Helmholtz vortices. Slow ablation (figure 2b) causes an intensification of the near-wall vortices close to the ablative wall. The boundary layer remains attached to the moving wall. Figure 3 compares velocity statistics for figures 2a and 2b to the corresponding statistics in channel flow at the same Reynolds number and two non-moving walls. Here the superscript  $+$  denotes the normalization of velocity and spatial coordinates by  $u_{\tau 0}$  and  $\nu$ . The vertical coordinate is normalized by  $h(t)$ , the height of the fluid domain at time  $t$ . The formation of the shear layer is obvious in the profile of mean shear (figure 3a). For slow ablation,

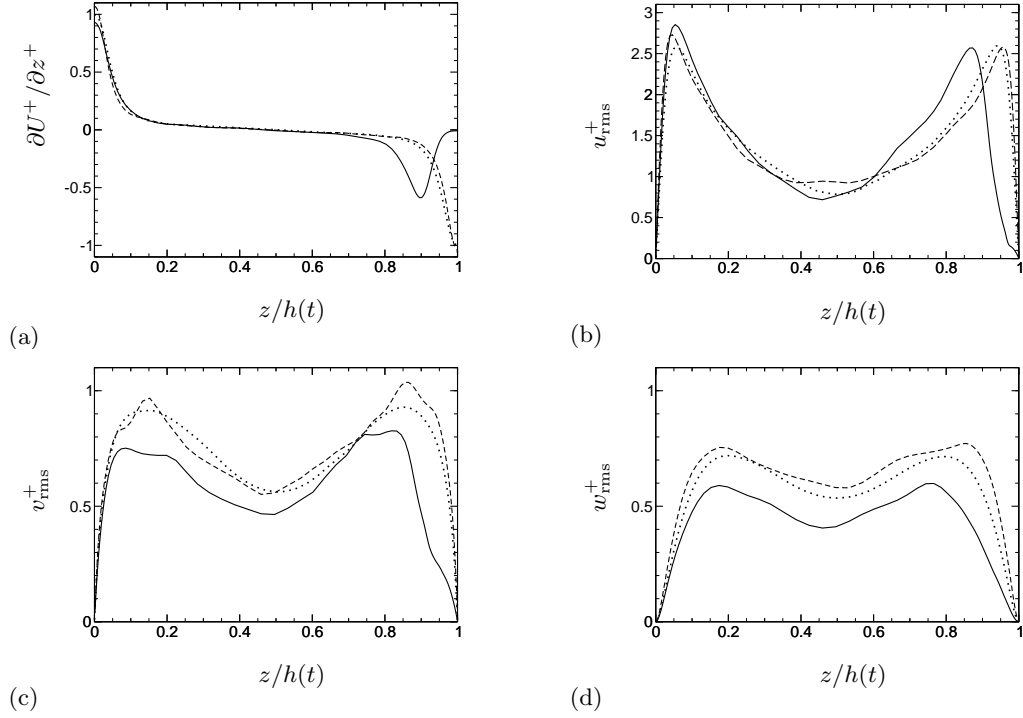


FIGURE 3. Velocity statistics corresponding to figures 2a (—,  $v_a = u_{\tau 0}$ ) and 2b (---,  $v_a = 0.01u_{\tau 0}$ ) compared to time and space-averaged statistics in a  $Re = 125$  channel flow with non-moving walls (⋯). The mean shear and root-mean-square of the stream-wise, span-wise, and vertical velocity fluctuations are shown in figures a,b,c,d, respectively.

the mean shear is very close to the reference. The statistical convergence of the rms of velocity fluctuations suffers from the small horizontal dimensions of our domain, yet they clearly indicate that (i) the slow ablation flow retains the turbulent structure observed at equilibrium and (ii) the effects of fast ablation mostly concentrated on vortical structures. Indeed, the maximum of  $u_{\text{rms}}^+$  (figure 3b) shows little difference from the reference. The location of this maximum is located very close to the original, i.e., before the onset of wall recession. Quasi-streamwise vortices govern the spanwise and vertical velocity fluctuations (figures 3c,d), which are both significantly reduced by fast wall recession.

### 3.2. Thermal ablation: challenges

The discussion here is focused on the identification and resolution of the challenges associated with the conjugate heat transfer and thermal ablation when the thermodynamical properties of the fluid and solid are vastly different. All simulations consist of a two dimensional natural convection using the following parameters:  $Ra = 1.05 \times 10^5$ ,  $Re = 125$ ,  $Pr_s = 10$ ,  $Pr_f = 0.7$ ,  $\kappa_s/\kappa_f = 5$ ,  $\rho_s/\rho_f = 1$ ,  $Ste = 10$ . The temperature boundary conditions are  $T_{\text{hot}} = 1.5$ , and  $T_{\text{cold}} = T_m = 0$ . The domain is  $L_x = 4$ ,  $L_z^{\text{channel}} = 2$ ,  $L_z^{\text{wall}} = 0.5$  with  $N_x = 64$ ,  $N_z^{\text{channel}} = 65$ ,  $N_z^{\text{wall}} = 250$  with a vertical stretching, where  $Ra$  is the Rayleigh number.

The conjugate heat transfer problem, i.e., in the absence of ablation, has the potential to cause large fluctuations of temperature close to the fluid-solid interface. Indeed, the difference in thermal conductivities between the two media, up to an order of magni-

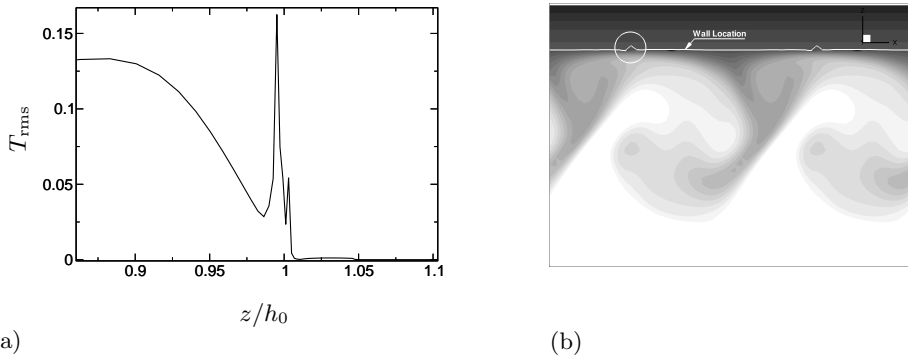


FIGURE 4. Example of unstable onset of ablation and its effect on temperature fluctuations in a 2D natural convection. Figure (a) The near-wall profile rms of temperature fluctuations averaged in the  $x$  direction and figure (b). The contours of temperature and the fluid-solid interface.

tude, imposes a significant discontinuity in the normal derivatives across the fluid-solid interface. The time scale of temperature fluctuations in turbulent flows is commensurate to the time scale of turbulence, when the Prandtl number is close to 1 (Batchelor 1959). Consequently, flow structures that create momentum fluxes toward the wall, vortices and/or convection cells also generate wall heat flux fluctuations on the same time scale. However, the time scale of temperature fluctuations is much longer in the solid due to thermal inertia. It is therefore not surprising that the coupling of conjugate heat transfer with immersed boundary methods could generate errors if the different time scales and boundary conditions are not solved adequately. The sudden increase of wall temperature in the downwash of a quasi-streamwise vortex or convection cell is of a convective nature, and the stability of the solution relies on the Courant Fredrichs Levy condition (CFL). By construction, the immersed boundary method modifies the nodes in the immediate vicinity of the wall to impose the local boundary condition using nodes further away as reference. An issue arises when the IBM attempts to correct the temperature in the solid, which is a diffusive process, on the same time scale as the flow. It is imperative that the diffusive term in the heat equation (Eq. 2.2) be treated implicitly in all directions. The potential for large discontinuities in temperature gradients across the interface also requires special treatment. The most robust solution is to recalculate the metrics used in the diffusive term for nodes at or close to the interface as a function of the thermal boundary conditions to be imposed at the interface. Conceptually, this is achieved using nodes directly across the interface as virtual ghost nodes on which the proper thermal boundary conditions are interpolated. The solution is then iterated until the error on the temperature field is less than a given absolute tolerance. We used  $10^{-6}$  since lower tolerance did not change solutions appreciably.

While this methodology proves to be stable for pure conjugate heat transfer problems, it was still found to cause local errors inducing unstable behaviors when ablation occurs. An example of such behaviors is shown in figure 4. Large variations in the fluctuations of temperature close to the interface are shown in figure 4. Here the RMS of temperature fluctuations are calculated from averaging in the  $x$  direction the two-dimensional natural convection flow displayed in figure 4b. These fluctuations create rapid changes in the sign of the temperature gradient around the interface. In the absence of ablation, these oscillations may exist without noticeably affecting the velocity field due to the strength of viscous dissipation at the wall. In the case of ablation, these errors have dire consequences

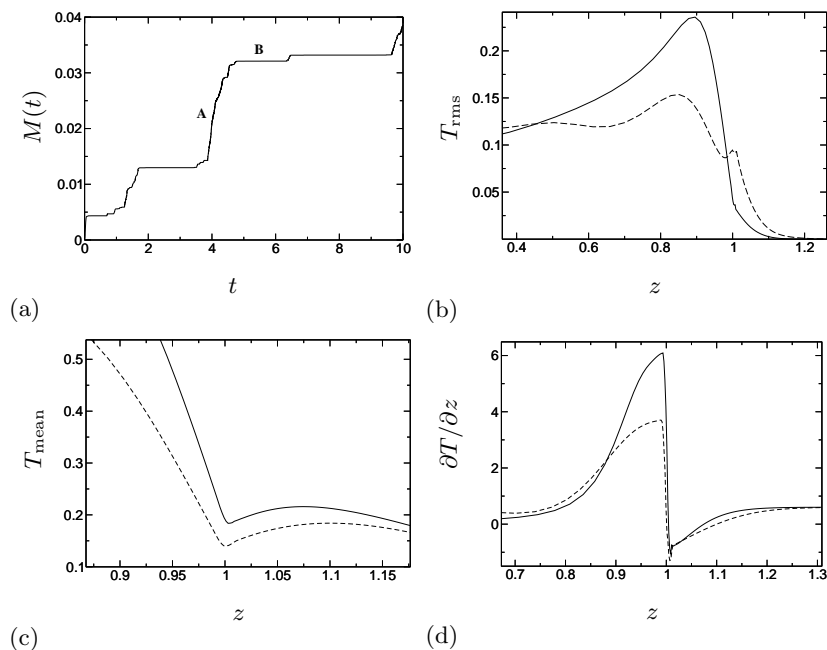


FIGURE 5. Example of onset of ablation by a two-dimensional natural convection flow. (a) The amount of total wall mass lost due to ablation as a function of time. A and B denote two examples of fast and slow ablation rates. Figures (b-d). The spatial profile of the rms of temperature fluctuations, the mean temperature and the vertical temperature derivative, respectively, close to the interface located in the vicinity of  $z = 1.0$ , rms of temperature near the wall. Figures (b-d), — corresponds to event A and ---- to event B.

on the stability of the solution since they directly enter the computation of the ablation velocity  $v_a$  (Eq. 2.9). The ablation velocity may easily reach unphysical speeds, orders of magnitude larger than realistic speeds. Since conservation of mass imposes that the fluid velocity at the wall be the opposite of  $v_a$ , the flow sees nodes where ablation velocity is too large as a discontinuity of  $f_i^{\text{ibm}}$  (Eq. 2.4) and the velocity field may diverge.

The solution is to implement a control loop on the calculation of the ablation velocity. First, the time-step is computed from the CFL constraint. This time-step is used to estimate ablation velocities at the interface. The maximum ablation velocity is then used to impose to  $\Delta_{\text{min}} / \max(v_a) \leq \Delta t$ , which amounts to a CFL=1 condition on the ablation velocity since  $\Delta_{\text{min}}$  is the grid spacing along the direction of  $\max(v_a)$ . If the test fails, the time-step is divided by 10, and ablation velocities are estimated again. Typically, large Stefan number ( $Ste = 10$ ) requires a division by a thousand of the time-step over 100 to 1000 iterations. By monitoring  $\max(v_a)$ , we were able to confirm that the constraint is physics-based, not induced by numerical errors. For instance, if the first estimate of  $\max(v_a)$  is of the order of 10, the second (with  $\Delta t/10$ ) is unchanged, and neither is the third ( $\Delta t/100$ ). Since our time advancement is at the minimum of second order, a numerical error would have resulted in a continuous decrease of  $\max(v_a)$  with the reduction of the time-step.

### 3.3. Thermal ablation: Example

Upon implementation of the virtual ghost point method for the thermal immersed boundary methods and the control loop on the time-step, the algorithm was tested in several

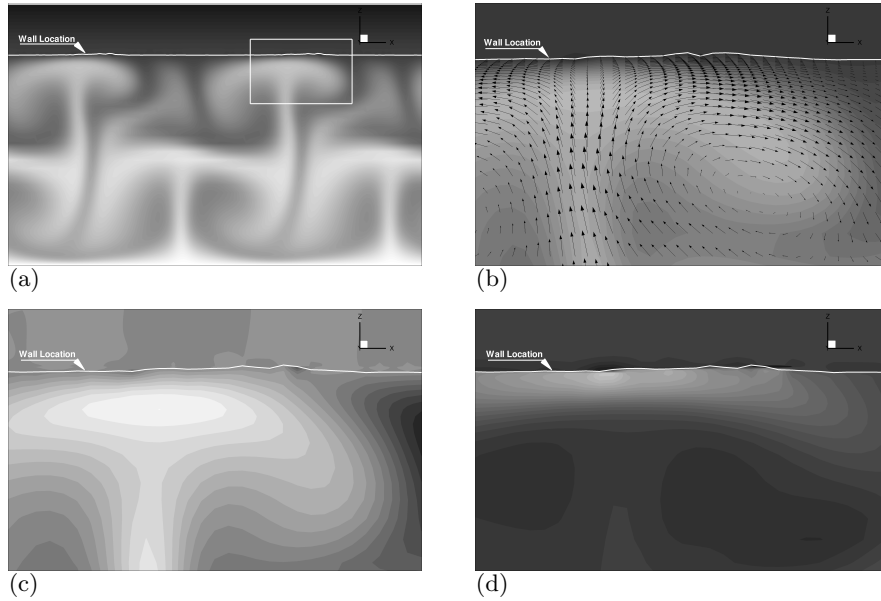


FIGURE 6. Snapshots of 2D natural convection where (b),(c),and (d) are close-up images taken inside the outline rectangle in (a). (a) Temperature contours of 2D natural convection with ablation. (b) Temperature contours and velocity vectors near the ablated wall. (c) Fluctuating temperature,  $T'$ , near the ablated wall. (d)  $\partial T/\partial z$  near the ablated wall.

configurations. Here we report an onset of ablation caused by a two-dimensional convection flow. figure 5a reports the evolution of the mass of solid ablated as a function of time. The ablation rate is intermittent, fast over a very short period of time and slow over longer durations. Figures 5b-d describe the rms of temperature fluctuations, mean temperature and vertical temperature derivative for rapid (event A in figure 5a) and slow ablation rates (event B). Quantities are averaged in  $x$ . These figures highlight the stiffness of the thermal problem close to interface, in particular the discontinuity of the temperature derivative. As the ablation proceeds, we observe the emergence of small-scale roughness in the interface (figure 6). Although modest, the topology of the wall shares some similitude with "sharkskin" observed in Sugawara *et al.* (2007). Figure 6, and figures. 6b-d show a zoom-in of the velocity field and contours of temperature, temperature fluctuations and fluctuations of the vertical temperature derivative. Future studies will focus on the dynamics and predictability of the interface topology

#### 4. Conclusion

An algorithm for the direct numerical simulation of a turbulent flow over a receding wall was discussed. A numerical experiment was used to quantify the non-equilibrium effects in a periodic channel flow with one receding wall. Fast recession causes the detachment of the boundary layer on the receding wall and the formation of shear layer flow. Slow recession, 1% of the skin-friction velocity before onset of recession, maintains the equilibrium structure of the turbulent flow. Thermal ablation was studied in the context of sublimation, with additional approximations, such as Boussinesq approximations and incompressibility. The goal was to test the algorithm used to define the fluid-solid interface, which combines level-set and immersed boundary methods. Of the many challenges

encountered, the two principal problems, computation of temperature derivatives at the interface and resolution of large ablation velocity, were resolved. For the latter, a control loop on the determination of the time-step was implemented as a function of a CFL condition based on the maximum ablation velocity. An example of thermal ablation by natural convection is briefly discussed. The remaining challenge is in the discretization and re-initialization of the level-set methods. The strategies initially chosen, using standard ENO-type numerical schemes, were found to be too unstable for our flows. New numerical schemes have been implemented and are currently being tested, using higher-order methods and fast-marching methods. Publication of the validation of the algorithm and results is forthcoming.

### Acknowledgments

The authors are grateful for the support of National Science Foundation (CBET-0967857) and computational support from the Vermont Advanced Computing Center. The authors would also like to thank Dr. Olivier Desjardins for his guidance on level set methods and for sharing his fast marching method subroutine.

### REFERENCES

- BATCHELOR, G. K. 1959 Small-scale variation of convected quantities like temperature in turbulent fluid part 1. general discussion and the case of small conductivity. *J. Fluid Mech.* **5** (01), 113–133.
- DUBIEF, Y., TERRAPON, V., WHITE, C., SHAQFEH, E., MOIN, P. & LELE, S. 2005 New answers on the interaction between polymers and vortices in turbulent flows. *Flow, Turbulence and Combustion* **74** (4), 311–329.
- KANG, S., IACCARINO, G. & HAM, F. 2009 DNS of buoyancy-dominated turbulent flows on a bluff body using the immersed boundary method. *J. Comp. Phys.* **228** (9), 3189–3208.
- KIM, J. & MOIN, P. 1985 Application of a fractional-step method to incompressible Navier-Stokes equations. *J. Comp. Phys.* **59**, 308–323.
- MITTAL, R. & IACCARINO, G. 2005 Immersed boundary methods. *Annual Review of Fluid Mechanics* **37**, 239–261.
- MOHD-YUSOF, J. 1997 Combined immersed boundaries/B-splines methods for simulations of flows in complex geometries. *Center for Turbulence Research Annual Research Briefs NASA Ames/Stanford University*.
- MOIN, P. & IACCARINO, G. 2007 Complex Effects in Large Eddy Simulations. *Lecture Notes In Computational Science And Engineering* **56**, 1.
- OSHER, S. & SETHIAN, J. 1988 Fronts propagating with curvature-dependent speed: Algorithms based on Hamilton-Jacobi formulations. *Journal of Computational Physics* **79**, 12–49.
- SUGAWARA, M., TAMURA, E., SATOH, Y., KOMATSU, Y., TAGO, M. & BEER, H. 2007 Visual observations of flow structure and melting front morphology in horizontal ice plate melting from above into a mixture. *Heat and Mass Transfer* **43** (10), 1009–1018.
- TSENG, Y. FERZINGER, F. 2003 A ghost-cell immersed boundary method for ow in a complex geometry. *J. Comp. Phys.* **192**, 593–623.